Fracture Behavior and Damage Development in Self-Reinforced PET Composites Assessed by Located Acoustic Emission and Thermography: Effects of Flame Retardant and Recycled PET

G. Romhány[a], C. M. Wu[b], W. Y. Lai[b]and J. Karger-Kocsis[a,c*]

[a] Department of Polymer Engineering, Faculty of Mechanical Engineering, Budapest University of Technology and Economics, Muegyetem rkp. 3., H-1111 Budapest, Hungary
[b] Department of Materials Science and Engineering, National Taiwan University of Science and Technology, Taipei 10607, Taiwan, Republic of China
[c] MTA-BME Research Group for Composite Science and Technology, Muegyetem rkp. 3, H-1111 Budapest, Hungary

*corresponding author: karger@pt.bme.hu

Submitted to Compos. Sci. Technol., April, 2016, and revised May, 2016.

Abstract
Self-reinforced polyethylene terephthalate (srPET) composites were produced by hot pressing from woven fabrics composed of double covered uncommingled yarns. The mid section of the latter contained recycled PET homopolymer filaments (reinforcement) whereas the covering filaments (overtaking the role of the embedding matrix) were spun from a PET copolymer with and without flame retardant. The fracture of the srPET was studied in tensile loaded notched specimens using located acoustic emission (AE), infrared thermography (IT) and visual inspection in situ. The crack growth was reconstructed by evaluating the located AE and IT results and compared with the observed one. In the knowledge of the crack propagation the J-integral resistance (J_R) fracture mechanics concept was followed to characterize the fracture behavior. srPET with fire retardant matrix exhibited lower J_R characteristics than the unmodified composite. This was traced to differences in the failure modes considering the amplitude distribution of the AE events and post mortem failure analysis. Size of the damage zone was estimated by considering the located AE (≈20 mm) and IT results (≈15 mm), and the related difference discussed.

Key words:
A. Fabrics/textiles
A. Polymer-matrix composites (PMCs)
B. Fracture toughness
D. Acoustic emission

D. Non-destructive testing

1. Introduction

Self-reinforced composites are defined as composites in which the reinforcing and matrix phases are composed of the same polymer. A less strict definition refers to such polymers which belong to the same polymer family [1]. In the former case the processing window for consolidation, whereby wetting of the reinforcement by the matrix melt occurs, is very narrow because only the difference in the melting behavior between the isotropic matrix and strongly anisotropic reinforcing polymer can be exploited. Nonetheless, it has been proved as feasible for many polymers via the hot compaction method developed by Ward and coworkers [1, 2]. The processing window is markedly widened when the matrix giving material is a copolymer. Copolymers of random or block structures may exhibit markedly lower melting temperature than the homopolymer. Accordingly, homopolymer in different forms (fiber, tape and related assemblies) may serve as reinforcement whereas copolymer overtakes the role of the embedding matrix. This copolymer/homopolymer combination for the matrix/reinforcement of self-reinforced polymer composites (srPCs) is very promising for industrial production. This strategy has been followed for sr polypropylene (srPP) which is commercialized under the trade name PURE [1, 3]. PURE is a coextruded, stretched srPP tape having a copolymer/homopolymer/copolymer lay-up in which the major cross-sectional component is the homopolymer. The corresponding srPP composites are produced directly from tapes (winding, layer deposition) or by hot pressing from textiles composed of tapes (e.g. woven fabrics) [4].

Textile technologies are very versatile allowing us to produce different prefabricates for consolidation via hot pressing. This development was fueled by existing commingling strategies. Here traditional reinforcing fibers (glass, carbon) were mingled with thermoplastic polymer fibers which overtake the role of the matrix during consolidation. Complete impregnation of these hybrid rovings or yarns to produce void-free composites is a challenge. Fibers lying in the mid-section of such prefabricates should undergo melting and participate in the micro-infiltration process [5]. To avoid this, it seems to be a straightforward strategy to place the matrix-giving fibers on the surface of the reinforcing fibers by suitable techniques. This can be achieved by special textile wrapping methods, such as single or double covering of an uncommingled roving or yarn [6]. Note that for the cover wrapping copolymer, whereas for the core roving or yarn homopolymer fibers with suitable cross-section (fineness) should be used. A further benefit of this technique is that the higher melting core polymer fibers may be with (yarn) or without twisting (roving) to control their load bearing capability. It is noteworthy that these uncommingled wrapped rovings and yarns can be converted easily in various textile architectures, such as woven fabrics. The concept of this wrapped uncommingled preform is somewhat similar to that of PURE with the exception that the former is a non-consolidated (reinforcement not wetted out by the matrix), whereas the latter is a consolidated (intimate contact between matrix and reinforcement) preform of srPCs [1, 7]. In this respect credit has to be given to Karger-Kocsis who claimed that all production routes of thermoplastic matrix-based composites use either consolidated or non-consolidated preforms [7].

srPP composites are intensively studied as reviewed in Ref. [1]. Recently, even their flame retardance came under spot of interest due to further potential applications [8]. However, the thermal stability and thus the highest service temperature of srPP composites are low. This is the major reason why research and development works are devoted to produce srPCs using polymers of high temperature resistance [1]. Among the latter polyethylene terephthalate (PET) is preferred [9-11]. Its selection is reasoned also by the fact that the simplest economic recycling

of PET-based soft drink bottles is to convert them into textile fibers [12]. As a consequence, many textile products already contain recycled PET (rPET) fibers.

Previous works on srPCs underlined that they may exhibit excellent mechanical properties including high impact resistance and toughness [1, 6, 13]. On the other hand, their fracture behavior was scarcely studied by using fracture mechanical approaches [14]. The same note holds also for the assessment of the damage development and growth in srPCs [15, 16]. In order to deduce fracture mechanical parameters the crack tip growth should be followed which is not an easy task in highly ductile textile-reinforced thermoplastic composites. For this purpose processing of the located acoustic emission (AE) and analysis of the infrared thermographic (IT) pictures proved to be valuable tools [17, 18].

This work was aimed at studying the fracture mechanical performance of srPET composites with and without flame retardant containing rPET as reinforcement in 53 vol%. srrPET composites were produced by hot pressing a woven fabric composed of double covered uncommingled yarns. To determine the J-integral resistance curves (J_R) the crack growth has been tracked by location of AE, IT and pictures' sequence taken by webcam. The development of the damage zone size was estimated based on located AE and IT frames. Note that due to a change in the size of damage zone upon loading of textile-reinforced thermoplastic composites the resistance curve concepts of fracture mechanics should be followed [15, 19, 20].

2. Experimental section

2.1. Materials, yarns and fabrics

In this study PET (rPET) and flame retarded (FR) PET yarns (rPET-FR) spun from recycled soft drink bottles were used as reinforcements. These rPET and rPET-FR yarns consisted of 111 tex multifilament bundles exhibiting tenacity of 65.4 g/tex and 58.3 g/tex, and elongation of 25.3% and 27.4%, respectively. Every multifilament bundle contained 192 filaments.

Yarns of PET copolymer with and without FR (mPET-FR and mPET, respectively) served as matrices after hot pressing in the corresponding self-reinforced PET composites. These mPET and mPET-FR yarns consisted of 35.6 tex multifilament bundles with a tenacity of 42.8 g/tex and 21.6 g/tex, and elongation of 27.9% and 34.1%, respectively. The mPET and mPET-FR bundles contained 96 and 72 filaments (F), respectively. The specification of the yarns is given in Table 1. The melting temperature of the PET versions was determined in differential scanning calorimetry (DSC). The melting temperatures of the matrix-giving and reinforcing yarns were at 226 and 260°C, respectively. The amount of the phosphorous flame retardant was set at 5500 ppm.

Table 1. Specification of reinforcing and matrix-giving PET yarns

Material	Fineness/filament	Content of flame retardant	Strength (g/tex)	Elongation (%)	Melting temperature (°C)
rPET	111 tex/192 F	-	65.4	25.3	262
mPET	35.6 tex/96 F	-	42.8	27.9	226
rPET+FR	111 tex/192 F	5500 ppm	58.3	27.4	259
mPET+FR	35.6 tex/72 F	5500 ppm	21.6	34.1	227

2.2. Preparation of double covered uncommingled yarn (DCUY) and basket fabric thereof

The rPET and mPET yarns were combined in double covered uncommingled yarns by

hollow spindle spinning machine. This DCUY consisted of two components, viz. core and binding yarn. rPET yarn was used as core yarn whereas mPET as binding yarn. The schematic of the DCUY process is shown in Fig. 1. To obtain an even distribution of the reinforcing fibers the fiber volume fraction of reinforcing PET was set for ca. 53 vol% in this DCUY "preform". This was achieved by suitable selection of the spinning parameters, including number of turns (694 turn/meter), machine rotation speed (5500 rpm.) and machine output (7.93 m/min).

DCUY was used as a feed material for the production of 2/2 basket-woven fabric that fabricated by rapier weave machine. The density of wrap and weft was 13.4 bundles/cm and 11.8 bundles/cm, respectively.

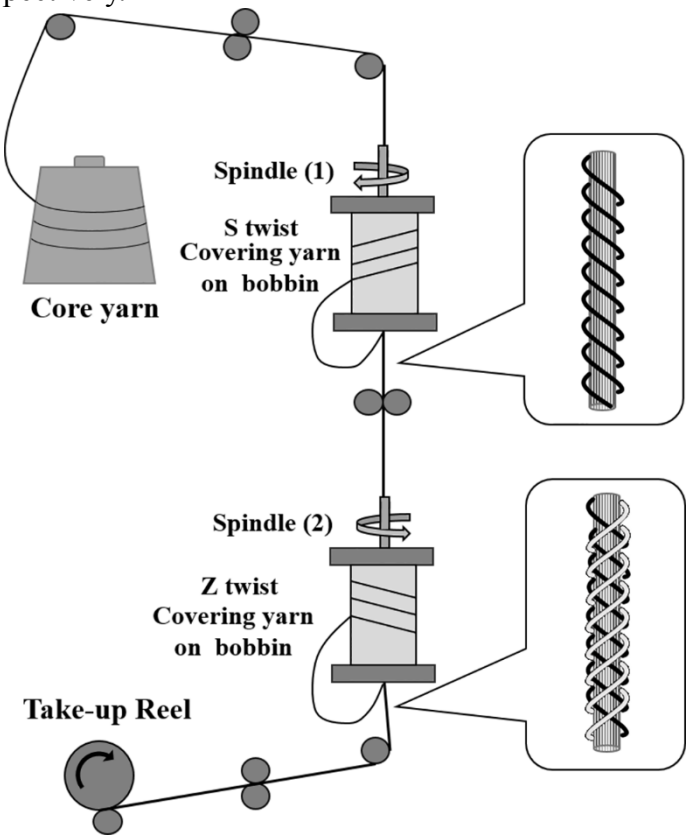

Fig. 1. Scheme of the DCUY production

2.3. Preparation and properties of self-reinforced PET composites

Two kinds of material systems were investigated, one is recycled self-reinforced PET composites (srrPET) and the other is recycled self-reinforced PET composites with flame retardant composites (srrPET-FR). The srrPET composites were fabricated in an industrial-scale hot press in a dimension of 1x1 m (FC-650TON, Long Chang, Taiwan). srrPET composites were prepared by stacking five layers of the basket fabrics and subjecting the related "package" to 12 MPa pressure at 235 ℃ for 1 minute that was followed by fast cooling. The thickness of the srrPET composites was 2 mm. Thanks to this high consolidation pressure the void content of srrPET composites was less than 1 % based on density measurements (ASTM D2734). Light microscopic pictures (BHZ-UMA, Olympus, Japan) taken on the polished cross-sections of sliced srPET composites confirmed the good consolidation quality achieved under the above-mentioned processing parameters. This is shown on example of the srrPET specimen in Figure 2. The appearances of the DCUY, basket fabric preform and the srrPET composite sheet are displayed in Figure 3.

In order to support the comparison of the reader with other srPCs the mechanical properties of the srPET composites produced are summarized in Table 2.

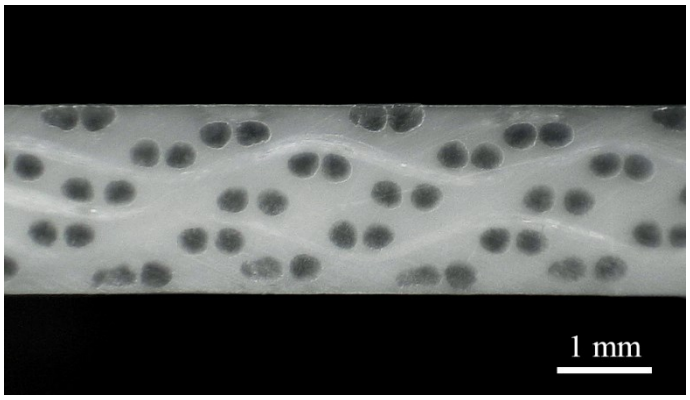

Fig. 2. Typical light microscopic picture taken on the polished cross-section of srrPET composite

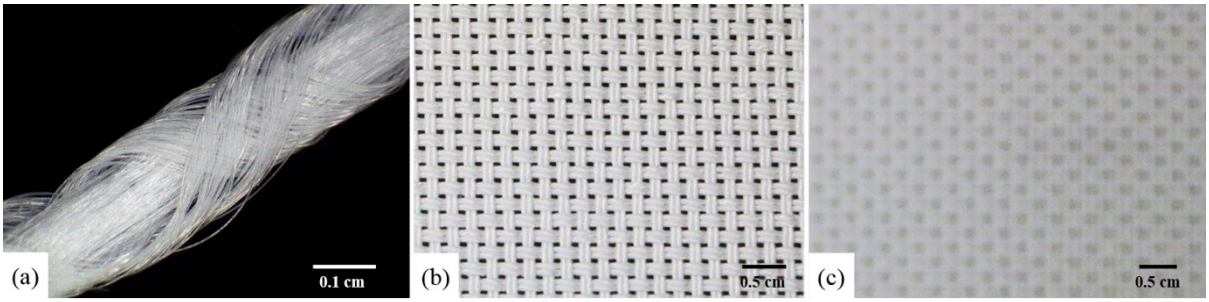

Fig. 3. DCUY yarn (a), 2/2 basket weave (b) and the corresponding srrPET composite

Table 2. Tensile properties for the srrPET and srrPET+FR composites. Because the stress-strain curves of the specimens showed two linear sections, well separated by a knee point (termed as to yield), the corresponding results are also given [21]

Sample	Tensile strength (MPa)	Tensile strain (%)	Tensile modulus (GPa)	Yield strength (MPa)	Post-yield modulus (MPa)
srrPET	121.3±1.8	24.4±0.7	3.4±0.1	41.0±1.3	323 ±5
srrPET+FR	110.7±6.6	16.5±0.8	3.8±0.2	41.6±2.0	467±60

The limiting oxygen index (ASTM D2863) values of srrPET and srrPET-FR where 26.6 and 35.3 %, while their UL-94 rating (ASTM D2863, vertical burning) V-1 and V-0, respectively.

2.4. Testing

2.4.1. Mechanical tests with AE recording

Static mechanical tests were performed on single edge-notched tensile loaded (SEN-T) specimens. Specimens with dimensions of 140 x 70 x 2 mm (length x width x thickness) were used. Chosen dimension of the SEN-T specimen allowed the location of the AE through a four sensors array (cf. Figure 4). Tensile loading of the SEN-T specimens occurred at room temperature at a deformation rate of 5 mm/min on a Zwick Z250 machine (Zwick GmbH, Ulm, Germany). The force vs. displacement curves were recorded during the tests. The initially

sawed notch (a_0) was sharpened by a fresh razor blade. It is noteworthy that the composites composed of five layers of the basket fabrics (exhibiting balanced and "dense" structure) already ensured a homogeneous stress (re)distribution and thus no effect of the notching was observed. The AE activity was recorded in situ during loading by a Sensophone AED-40 device (Sensophone Kft., Budapest, Hungary). A four sensor quadratic array, as shown in Figure 4, served to locate the AE events using wide bandwidth (100–600 kHz) microsensors (10 mm diameter, Micro 30D of Physical Acoustic Co., Princeton, USA). The signals were logarithmically amplified. As reference voltage 1μV was selected and the threshold was fixed at 30 dB. Tests were run on three specimens in order to check whether or not the results can be considered as characteristic ones.

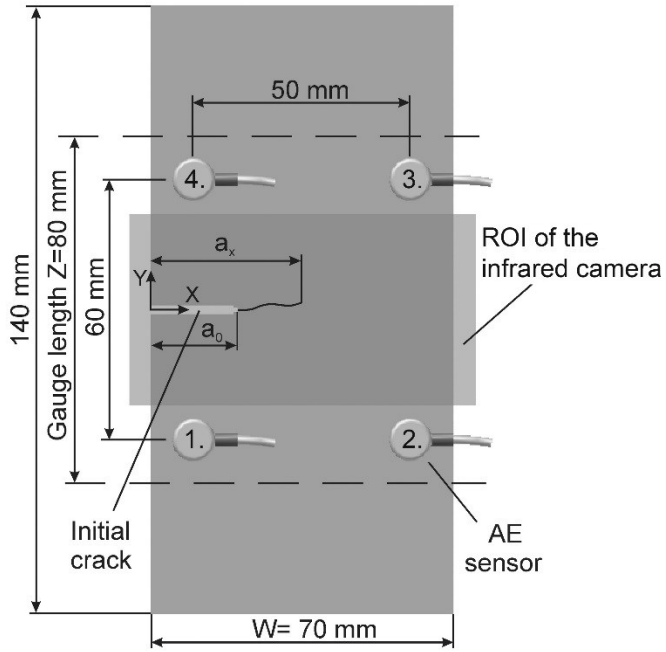

Fig. 4. Experimental set-up including the dimension of the SEN-T specimen, positioning the AE sensors and region of interest (ROI) field of the infrared camera.

Location occurred by a built-in algorithm of the device in the knowledge of the acoustic wave speed. The measurement of acoustic wave speed was determined by the method depicted in Figure 5. One sensor worked as transmitter and two others as receivers. Knowing the distance of the receivers from one another and difference in the arrival times of AE signal to the receivers the acoustic wave speed was calculated.

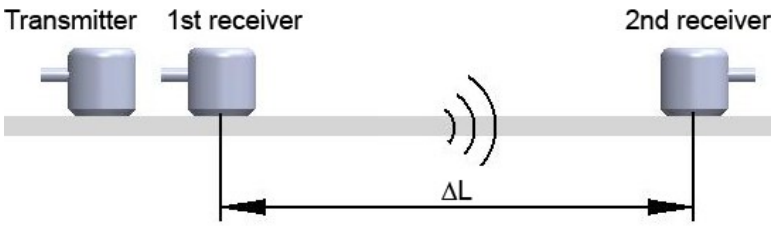

Fig. 5. Determination of the speed of the acoustic wave in the composites

Though the linear densities of wrap and weft bundles were similar, the fabric reinforcement – also due to the processing – may be anisotropic. Therefore no average AE wave speed was used. Instead the acoustic wave speed was measured between the 1-2, 1-3 and 1-4 sensor pairs and

set in the software. The mean values of the acoustic wave speeds between the sensors are given in Table 3.

Table 3. Measured acoustic wave speed between the sensors

	Mean acoustic wave speed (m/s)		
Sensor pairs	1-2	1-3	1-4
srrPET	2150	1700	1850
srrPET+FR	2050	1650	1800

2.4.2. Infrared thermography

The temperature rise of the specimens was measured by a FLIR A325sc infrared camera (FLIR Systems, Wilsonville, OR, USA). The apparatus has a working range -20°C and 350°C with an accuracy of ±2°C and provides pictures with a resolution of 320x240 pixels. The software stores the temperature of every pixel in a frame sampled with a preset frequency (30 Hz). This allows us post processing of the measured data.

2.4.3. Crack growth and fracture

Tracing of the crack growth was also followed by a Logitech C525 webcam with a resolution of 640*480 pixels. The fracture surfaces of the SEN-T specimens were inspected with Olympus BX51M type optical microscope (Olympus GmbH, Hamburg, Germany) and in a Jeol JSM 6380LA type scanning electron microscope (SEM; JEOL Ltd., Tokyo, Japan). Prior to observation, Au/Pd alloy was sputtered onto the surface to avoid electrostatic charging.

3. Results and discussion

3.1. J-integral resistance curves (J_R)

Figure 6 shows a typical force-elongation curve on example of the SEN-T specimen of srrPET Note that its run is practically identical with that of unnotched specimens [21] confirming that the srrPET composites are notch insensitive. The phenomenon "yielding", mentioned in connection with the data in Table 2, occurs at about 2 mm elongation.

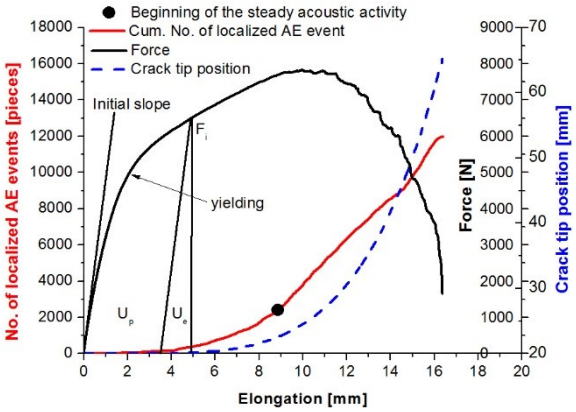

Fig. 6. Typical force-elongation trace measured on a SEN-T specimen of srrPET. Notes: this figure also shows how the elastic and plastic components of the J-integral have been determined at a given loading (F_i), more exactly at a given stage of the crack growth. Position of the crack tip is given based on the IT results (see later). The onset of "yielding" is marked by arrow.

The J_R curve is given by the actual J value plotted as a function of the crack advance (Δa), as shown later. Therefore the first task is to follow or to reconstruct the crack growth. The crack growth was followed by webcamera (visual inspection) and reconstructed based on the AE and IT results. In the two latter cases the located AE events and the IT frames, monitored as a function of time, were used as input parameters.
From the IT frames, grouped into consecutive decades, the position of the moving crack tip was determined as follows. From the heat map represented by the (i+1)th 10^{th} frame the ith 10^{th} was deduced. The related time interval corresponded to 2.66s. This difference in the corresponding heat maps was considered to reflect the heat development in the elapsed time thereby accepting adiabatic conditions. The actual crack tip position was estimated by the center of gravity of the heat map received and assigned to the mid time period (i.e. 1.33 s).
The crack path reconstruction through located AE events was similar as disclosed in detail in our previous paper [20]. Briefly, to assess the crack growth process identical time intervals with IT were selected. In these time intervals the center of gravity of the located AE events along the x-axis (free ligament, cf. Figure 4) were determined and its position was equaled with that of the actual crack tip in the mid time of the corresponding time interval (i.e. at 1.33 s). This estimation procedure differed somewhat from the earlier used one [20] since no attempt was made to determine by iteration that time interval which yields monotonous crack growth.

Position of the crack in a SENT-T specimen of srrPET, determined by different techniques, is depicted in Figure 7. Figure 7 shows that the crack positions, determined and deduced by different techniques agree reasonably well with each other.

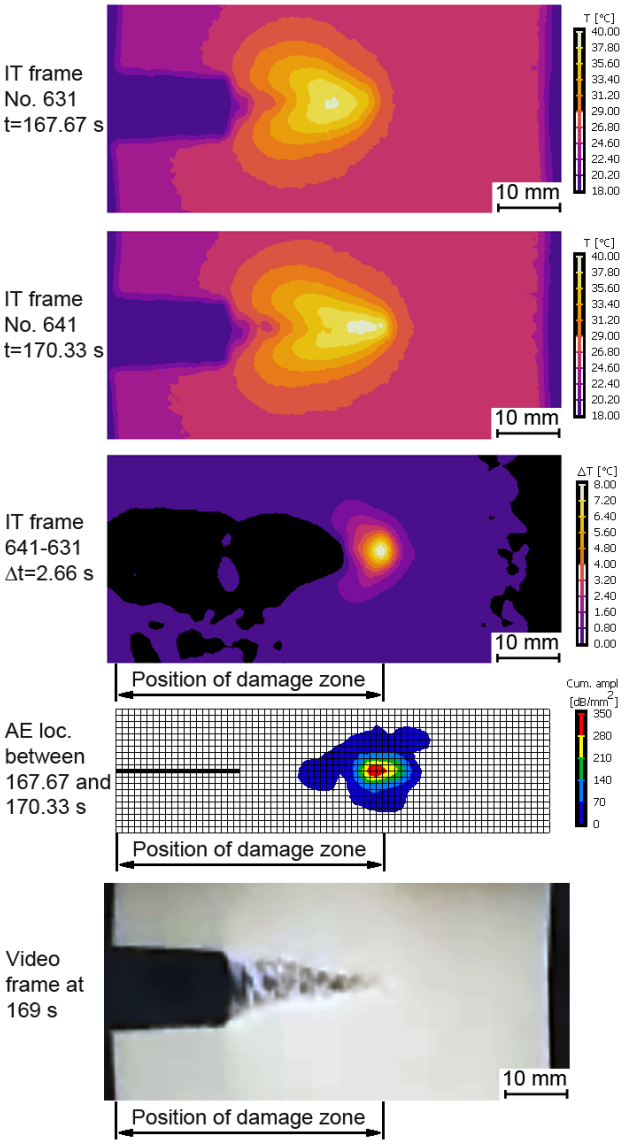

Fig. 7. Comparison of the crack positions, assessed by different techniques, at a given loading time period for srrPET. Notes: position by IT is given through the excess heat development in a given time interval. Position by AE was estimated by calculating the weight center of the positions of the located AE events in the same time interval than that of IT. The grid scale in the AE map corresponds to 1 mm. Picture by the web camera was taken in the mid part of the selected time interval

The crack advance, i.e. position of the crack tip along the free ligament (W-a_x; cf. Figure 4), estimated by the three different methods is depicted on example of srrPET in Figure 8.

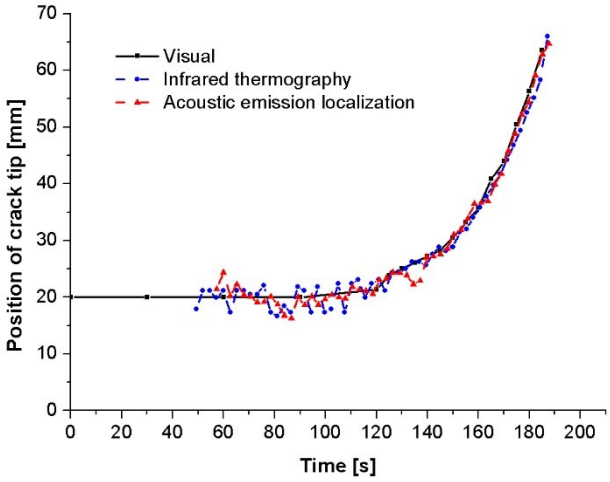

Fig. 8. Comparison of the crack tip positions, determined by different techniques, on example of srrPET

Based on the fact that the IT evaluation resulted in smaller scatter than AE, the former approach has been preferred further on. In order to determine the actual position of the crack tip - which is required for computing the J-integral (cf. Figure 6) - the IT-related experimental crack tip values were fitted by a four parameter Weibull-type function. So, the IT-related crack tip movement was approached by a four-parameter Weibull-type function, given in Equation 1:

$$a(t) = A - (A - a_0) \cdot e^{-(B \cdot t)^C}, \tag{1}$$

where a_0, A, B, C are parameters, a_0 equals with the initial notch length (cf. Fig. 4).

Resistance curve of the J-integral (J_R) informs us about the change of the energy required to produce unit cracked surface as a function of crack advance (Δa) along the free ligament of the specimen. This fracture mechanical approach is selected when the crack resistance of the material is expected to change through an alteration in the damage zone and/or failure mode within with progressing crack.
The J-integral was calculated via Equations 2-8 [22, 23]:

$$J = J_e + J_p, \tag{2}$$

$$J_e = \frac{\eta_e \cdot U_e}{B \cdot (W - a)}, \tag{3}$$

$$J_p = \frac{\eta_p \cdot U_p}{B \cdot (W - a)}, \tag{4}$$

where J_e and J_p are, respectively, the elastic and plastic components of the total J value, U_e and U_p are, respectively, the elastic and plastic components of the external work (cf. Fig.6), η_e and η_p are elastic and plastic work factors dependent upon the specimen geometry, W is the width of the SEN-T specimen, B is the thickness of the SEN-T specimen, a is the actual crack length (cf. Fig. 4).
The elastic and plastic work factors for the SEN-T geometry were calculated using [22]:

$$\eta_e = \frac{(W - a_0) \cdot Y^2(a_0) \cdot a_0}{\int_0^{a_0} Y^2(a) \cdot a \ \ da + \frac{Z \cdot W}{2}}, \tag{5}$$

$$\eta_p = \frac{(W - a_0)}{W \cdot \alpha(a_0) \cdot \left[\left(\frac{W - a_0}{W \cdot [\alpha(a_0) - (a_0 / W)]} \right) + 1 \right]^{-1}}, \tag{6}$$

where

$$\alpha = [1 - 2(a/W) + 2(a/W)^2]^{1/2}, \tag{7}$$

$$Y = 1.99 - 0.41 \cdot \left(\frac{a}{W}\right) + 18.7 \cdot \left(\frac{a}{W}\right)^2 - 38.48 \cdot \left(\frac{a}{W}\right)^3 + 53.84 \cdot \left(\frac{a}{W}\right)^4. \tag{8}$$

The J_R curves received are displayed in Fig. 9. From the J_R curves usually two parameters are determined: the critical J-integral and the tearing modulus. There are different methods to determine the critical J-integral value. In this work, the intersection of the linear part of the J_R curve with the y-axis (J_0 at $\Delta a = 0$) is given as critical values. For a given section of the J_R curves a linear relationship holds:

$$J = J_0 + \frac{\Delta J}{\Delta a} \cdot \Delta a, \tag{9}$$

where $\Delta J/\Delta a$ is the tearing modulus.
Note that the higher the values of J_0 and the tearing modulus the higher the resistance of the composite to crack growth and crack propagation, respectively.

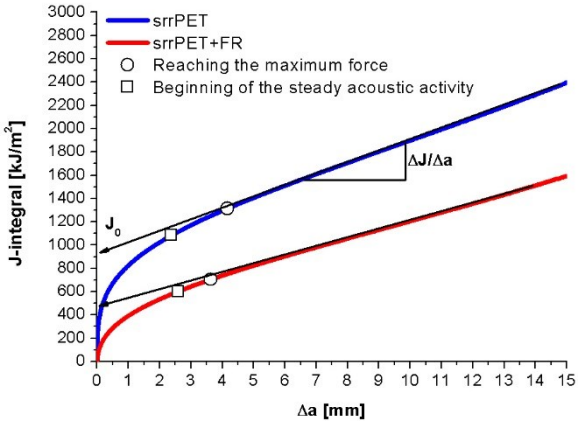

Fig. 9. Characteristic J_R curves of srrPET and srrPET+FR composites. Notes: in the traces the onset of steady acoustic activity (□) (cf. Fig. 6) and data points linked to the maximum load (o) are indicated.

One can see that the critical J values, irrespective of their determination methods, are higher for srrPET than srrPET-FR. srrPET has also somewhat higher tearing modulus than srrPET-FR. The related data are tabulated in Table 4. Accordingly, the introduction of FR reduced the resistance to fracture initiation and growth.

Table 4. Critical J-integral (J_0) and tearing modulus data for the composites tested. Note: data derived from three parallel tests

Material	J_0 (kJ/m^2)	$\Delta J/\Delta a$ (MJ/m^3)
srrPET	923 ± 94	105 ± 16
srrPET+FR	475 ± 103	87 ± 9

3.2. Damage growth and failure

Coming back to Figure 7 the size of the damage zone can be estimated based on the AE and IT results. Based on the located AE the size of the damage zone is at about 20 mm. Such large damage zones have been found for other fabric reinforced thermoplastics, such as glass fiber mat-reinforced PP [17-19]. Based on the differential IT frame, however, a bit smaller damage zone can be deduced, viz. at about 15 mm. It was argued [24] that this difference, which is always present, reflects the difference between the damage and plastic zone. The damage zone includes also such individual failure events which are not or less accompanied with heat development, such as debonding. By contrast, in the plastic (or active) zone such events dominate which work as prominent heat sources. The latter are: roving/fiber fibrillation and fracture, roving/fiber pull-out, and associated matrix deformation (crazing and shear yielding).

In order to get further insight in the failure mode selected parameters of the registered burst-type AE events were analyzed. Figure 10 a and b show that srrPET had higher AE activity than the companion srrPET-FR. To find its reason the AE amplitude distributions monitored up to final fracture were compared – cf. Figure 11. It is widely accepted that the AE amplitude range increases according to the following individual failure events: debonding< pull-out < fracture. The above ranking correlates well with the energy absorption of the corresponding failure events.
Figure 11 clearly show that considerably larger proportion of the AE events exhibits low amplitudes for srrPET-FR than for srrPET. This suggests the onset of debonding-type events obviously supported by the FR particles. It is noteworthy that fiber/matrix debonding is generally the first failure mode in all fiber-reinforced composites. High probability of debonding is usually a hint for low interphase adhesion between the matrix and reinforcement. Further on, the relative frequency of high amplitude AE signals is markedly more in srrPET than in srrPET-FR. These facts confirm that srrPET composites have higher resistance to crack initiation and growth compared to srrPET-FR.

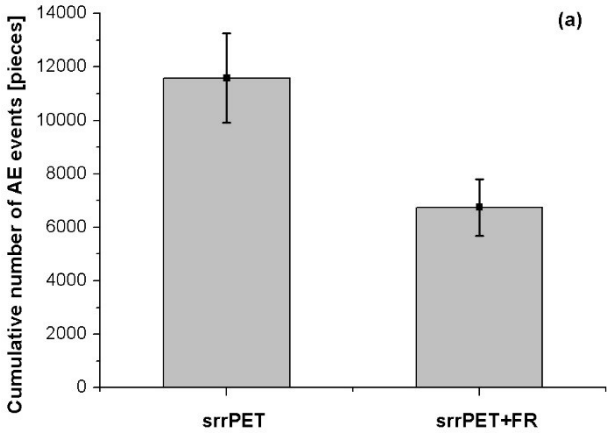

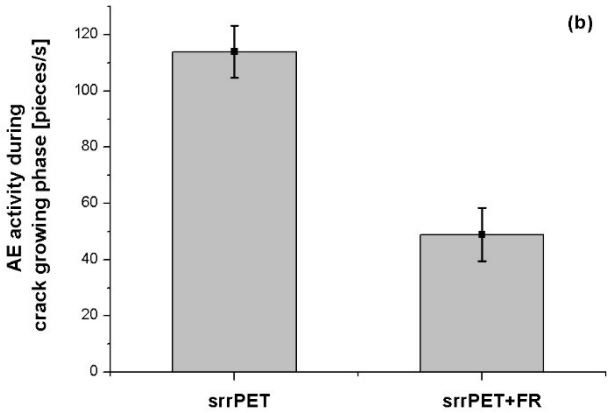

Fig. 10. a) Cumulative number of AE events, and b) emission speed of the AE monitored in the whole fracture process in srrPET and srrPET-FR composite specimens

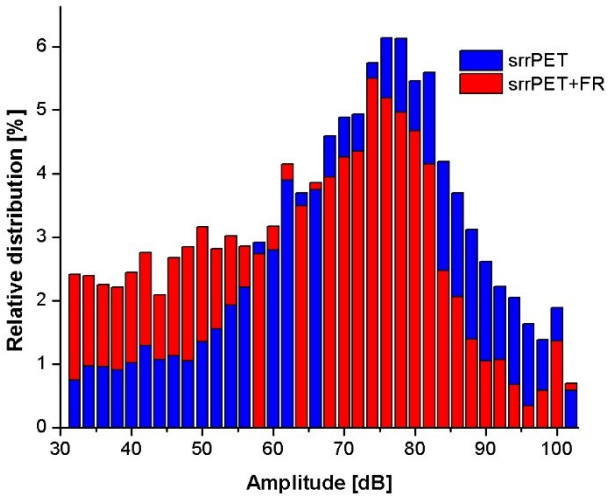

Fig. 11. Relative frequency of the amplitudes of the registered AE events in the whole fracture process of srrPET and srrPET-FR composite specimens. Note: characteristic feature without scatter range for sake of better comparability

In order to get a deeper insight in the failure mode the broken specimens were subjected to visual and microscopic inspections. The microphotographs in Figure 12 clearly show the difference in the fracture resistance of the composites tested. srrPET-FR is more easily fracturing than srrPET because the yarns are less fibrillated in the former case. Moreover, large scale yarn debonding occurs in srrPET-FR rather than in srrPET. Characteristic SEM pictures taken from the composites investigated are given in Figures 13-14. Comparing the pictures in Figure 13 a and b it is well resolved that the reinforcing PET filaments in srrPET are less bundled, i.e. the initial yarn structure is hardly observable, by contrast to srrPET-FR. This confirms already that srrPET should have higher resistance to fracture than srrPET-FR. Comparing the matrix- and interphase-related failures based on the SEM pictures in Figure 14 one is getting the major reason for the difference in the fracture behaviors of the composites tested. The FR particles cause secondary cracking owing to debonding in the PET copolymer matrix. This is well observable in the matrix failure mode showing residues of embryonal craze formation (arrows indicate in Figure 14 b). This feature is completely missing for srrPET. Moreover, according to a closer look the reinforcing homopolymer PET filaments are somewhat better adhered to the copolymer matrix (i.e. they are more covered) in srrPET than in srrPET-FR. All this information is in line with the fracture mechanics results obtained.

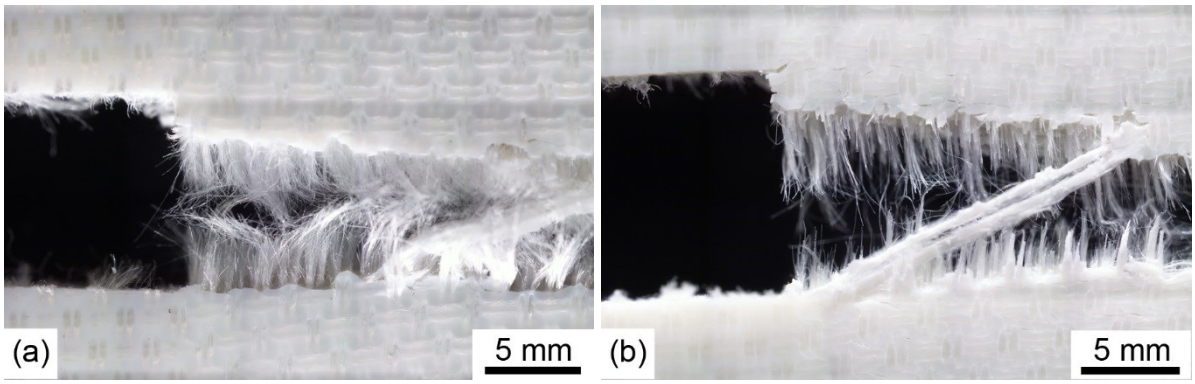

Fig. 12. Microphotographs taken from the surface of the SEN-T specimens of srrPET (a) and srrPET-FR (b), respectively

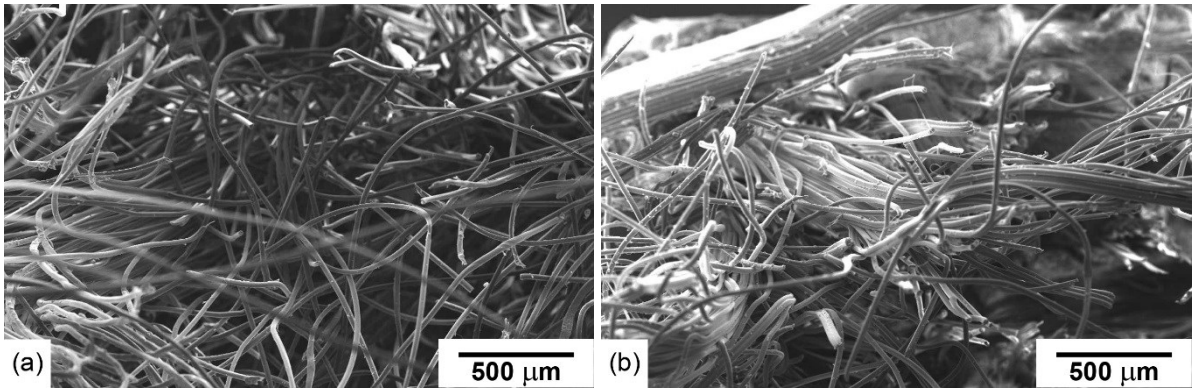

Fig. 13. SEM pictures taken from the fracture surfaces of the SEN-T specimens of srrPET (a) and srrPET-FR (b)

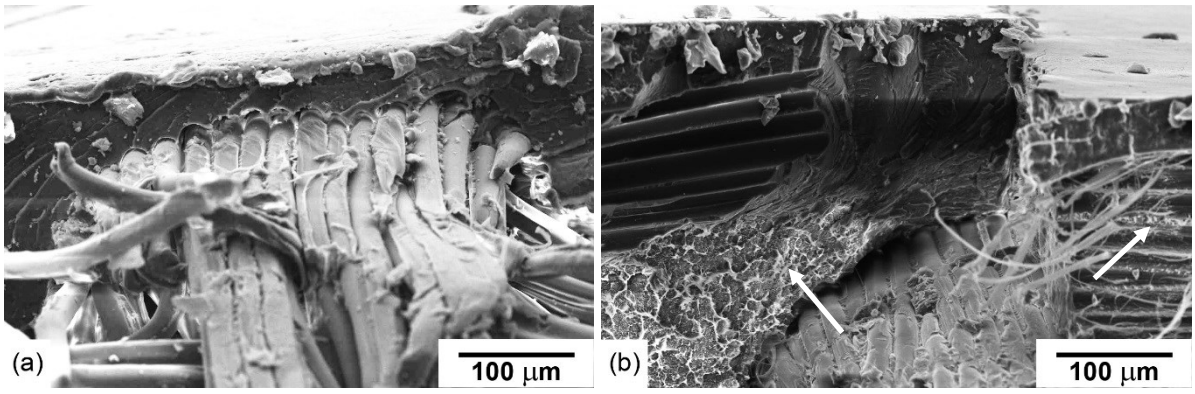

Fig. 14. High magnification SEM pictures taken from the fracture surfaces of the SEN-T specimens of srrPET (a) and srrPET-FR (b). Note: arrows indicate early stage craze formation

4. Conclusions

This work devoted to study the fracture mechanics performance, damage growth and failure characteristics of self-reinforced PET composites produced by hot pressing from a stack of fabrics woven from double covered uncommingled yarns. These yarns contained recycled PET homopolymer filaments onto PET copolymer filaments were wrapped. The latter, with and without flame retardant, served as matrix in the composites after hot pressing. Based on this study the following conclusions can be dawn:

- the crack path in the notched tensile loaded specimens could be properly reconstructed making use of the processing of the located burst-type acoustic emission (AE) events

(movement of the center of gravity of the AE events as a function of the) and infrared thermographic picture sequences (movement of the maximum temperature in differential heat maps as a function of time) because the estimated crack growth agreed very well with the visually observed one. This allowed us to adopt the J-integral resistance curve (J_R) concept of fracture mechanics for these self-reinforced composites.

- data deduced form the J_R curves differed for the self-reinforced PET composites depending whether their matrix contained flame retardant or not. Both the initiation J-integral and slope of the J_R curve were smaller for the flame retarded than for the reference composite. This difference was traced to alteration in the failure modes. Considering the AE amplitudes' distributions and fractographic results the flame retarded self-reinforced PET was more prone for interphase- and matrix-related debonding than the reference one.

References:

[1] J. Karger-Kocsis, T. Bárány, Single-polymer composites (SPCs): Status and future trends, Composites Science and Technology 92(0) (2014) 77-94.
[2] P. Hine, I. Ward, High stiffness and high impact strength polymer composites by hot compaction of oriented fibers and tapes, Mechanical properties of polymers based on nanostructure and morphology (2005) 683-727.
[3] B. Alcock, N.O. Cabrera, N.M. Barkoula, T. Peijs, Low velocity impact performance of recyclable all-polypropylene composites, Composites Science and Technology 66(11–12) (2006) 1724-1737.
[4] N. Cabrera, B. Alcock, J. Loos, T. Peijs, Processing of all-polypropylene composites for ultimate recyclability, Proceedings of the Institution of Mechanical Engineers, Part L: Journal of Materials Design and Applications 218(2) (2004) 145-155.
[5] J. Nunes, F. van Hattum, C. Bernardo, A. Brito, A. Pouzada, J. Silva, A. Marques, Production of thermoplastic towpregs and towpreg-based composites, in: K. Friedrich, S. Fakirov, Z. Zhang (Eds.), Polymer Composites: From Nano-to Macro-Scale, Springer, Berlin, 2005, pp. 189-213.
[6] C.M. Wu, P.C. Lin, C.T. Tsai, Fabrication and mechanical properties of self-reinforced polyester composites by double covered uncommingled yarn, Polymer Composites (2015).
[7] J. Karger-Kocsis, Composites (structure, properties, and manufacturing), Polymeric Materials Encyclopedia, CRC Press, Boca Raton, FL, USA, 1996, pp. 1378-1383.
[8] K. Bocz, A. Toldy, Á. Kmetty, T. Bárány, T. Igricz, G. Marosi, Development of flame retarded self-reinforced composites from automotive shredder plastic waste, Polymer Degradation and Stability 97(3) (2012) 221-227.
[9] P.J. Hine, I.M. Ward, Hot compaction of woven poly(ethylene terephthalate) multifilaments, Journal of Applied Polymer Science 91(4) (2004) 2223-2233.
[10] D. Yao, R. Li, P. Nagarajan, Single-polymer composites based on slowly crystallizing polymers, Polymer Engineering & Science 46(9) (2006) 1223-1230.
[11] J.C. Chen, C.M. Wu, F.C. Pu, C.H. Chiu, Fabrication and mechanical properties of self-reinforced poly (ethylene terephthalate) composites, Express Polymer Letters 5(3) (2011) 228-237.
[12] B. Geyer, G. Lorenz, A. Kandelbauer, Recycling of poly(ethylene terephthalate) – A review focusing on chemical methods, Express Polymer Letters 10(7) (2016) 559-586.
[13] Á. Kmetty, T. Bárány, J. Karger-Kocsis, Self-reinforced polymeric materials: A review, Progress in Polymer Science 35(10) (2010) 1288-1310.

[14] G. Romhany, T. Barany, T. Czigany, J. Karger-Kocsis, Fracture and failure behavior of fabric-reinforced all-poly (propylene) composite (Curv®), Polymers for Advanced Technologies 18(2) (2007) 90-96.
[15] X. Zhuang, X. Yan, Investigation of damage mechanisms in self-reinforced polyethylene composites by acoustic emission, Composites Science and Technology 66(3–4) (2006) 444-449.
[16] I. Halász, G. Romhány, Á. Kmetty, T. Bárány, T. Czigány, Failure of compression molded all-polyolefin composites studied by acoustic emission, Express Polymer Letters 9(3) (2015) 321-328.
[17] J. Karger-Kocsis, Z. Fejes-Kozma, Failure Mode and Damage Zone Development in a GMT-PP by Acoustic Emission and Thermography, Journal of Reinforced Plastics and Composites 13(9) (1994) 768-792.
[18] T. Czigany, J. Karger-Kocsis, Determination of the damage zone size in textile fabric reinforced polypropylene composites by locating the acoustic emission, Polymers & polymer composites 1(5) (1993) 329-339.
[19] O.I. Benevolenski, J. Karger-Kocsis, T. Czigány, G. Romhány, Mode I fracture resistance of glass fiber mat-reinforced polypropylene composites at various degree of consolidation, Composites Part A: Applied Science and Manufacturing 34(3) (2003) 267-273.
[20] G. Romhány, T. Czigány, J. Karger-Kocsis, Determination of J–R curves of thermoplastic starch composites containing crossed quasi-unidirectional flax fiber reinforcement, Composites science and technology 66(16) (2006) 3179-3187.
[21] C. Wu, W. Lai, Mechanical and open hole tensile properties of self-reinforced PET composites with recycled PET fiber reinforcement, Journal of Applied Polymer Science 133 (2016) 43682.
[22] A. Arkhireyeva, S. Hashemi, Determination of fracture toughness of poly (ethylene terephthalate) film by essential work of fracture and J integral measurements, Plastics, Rubber and Composites 30(7) (2001) 337.
[23] T.L. Anderson, Fracture Mechanics Fundamentals and Applications, second ed., CRC Press, Bota Raton, FL, USA, 1994.
[24] J. Karger-Kocsis, Swirl mat–and long discontinuous fiber mat–reinforced polypropylene composites—status and future trends, Polymer composites 21(4) (2000) 514-522.